

# V, J, H and K Imaging of the Metal Rich Globular Cluster NGC 6528 <sup>★</sup>

## Reddening, metallicity, and distance based on cleaned colour-magnitude diagrams

Y. Momany<sup>1</sup>, S. Ortolani<sup>1</sup>, E. V. Held<sup>2</sup>, B. Barbuy<sup>3</sup>, E. Bica<sup>4</sup>, A. Renzini<sup>5</sup>, L. R. Bedin<sup>1</sup>, R. M. Rich<sup>6</sup>, and  
G. Marconi<sup>7,8</sup>

<sup>1</sup> Dipartimento di Astronomia, Università di Padova, vicolo dell'Osservatorio 2, I-35122 Padova, Italy

<sup>2</sup> Osservatorio Astronomico di Padova, vicolo dell'Osservatorio 5, I-35122 Padova, Italy

<sup>3</sup> Universidade de São Paulo, Rua do Matao 1225, 05508-900 Sao Paulo, Brazil

<sup>4</sup> Universidade Federal do Rio Grande do Sul, Dept. de Astronomia, 91501-970 Porto Alegre, Brazil

<sup>5</sup> European Southern Observatory, Karl-Schwarzschild-Str. 2, D-85748 Garching, Germany

<sup>6</sup> UCLA, Department of Physics & Astronomy, 8979 Math-Sciences Building, Los Angeles, CA 90095-1562, USA

<sup>7</sup> Osservatorio Astronomico di Roma, Via dell'Osservatorio 5, I-00040 Monte Porzio, Italy

<sup>8</sup> European Southern Observatory, Alonso de Cordova 3107, Vitacura, Santiago, Chile

Received 27 August 2002 / Accepted .... 2002

**Abstract.** New near-infrared observations of NGC 6528 are presented. The  $JHK_s$  observations complement a previous HST/NICMOS data set by Ortolani et al. (2001), in that they sample a larger area, contain a more numerous sample of red giant stars, and include the  $K$  band. Also, archival HST data sets (separated by 6.093 years) were used to proper-motion decontaminate the near-infrared sample and extract a clean  $VJHK$  catalogue. Using the present wide colour baseline, we compared the cleaned colour-magnitude diagrams of NGC 6528 with those of NGC 6553 and NGC 104 and derived new estimates of reddening and distance,  $E_{B-V} = 0.55$  and  $(m - M)_0 = 14.44$  (7.7 kpc). Moreover, the morphology and location of the cleaned red giant branch were used to derive a *photometric* estimate of the cluster metallicity. The average of 10 metallicity indicators yields a mean value of  $[M/H] \approx 0.0$ , and  $[Fe/H] \simeq -0.20$  and  $+0.08$  on the Zinn & West (1984) and Carretta & Gratton (1997) revised metallicity scale, respectively. The best isochrone fit to the cleaned  $K, V - K$  diagram is obtained for a 12.6 Gyr and  $Z = 0.02$  isochrone, i.e. the derived metallicity of NGC 6528 turns out to be very close to the mean of stars in the Baade's Window. Five AGB variable star candidates, whose membership has to be confirmed spectroscopically, are bolometrically as bright as the known long period variable stars in NGC 6553. As discussed in Guarnieri et al. (1997) for NGC 6553, this may indicate that an "intermediate age" population is not needed to account for the brightest stars in external galaxies such as M32.

**Key words.** stars: fundamental parameters – stars: Population II – stars: late-type – individual: NGC 6528 – infrared: stars.

## 1. Introduction

The Galactic Globular Cluster (GC) system has long been used for investigating the early chemical evolution of the Milky Way. In particular, information regarding the spatial distribution, dynamical properties and chemical abundances of metal rich GCs constrain theories on the formation of the Galactic bulge, hence on the evolution of the Galaxy as a whole (Ortolani et al. 1995). There are 74

globular clusters projected within  $20^\circ \times 20^\circ$  of the Galactic center, among which 60 have galactocentric distances  $R_{GC} < 4$  kpc. In Barbuy et al. (1999) it was shown that most of these inner clusters have red Horizontal Branches (HB), whereas the fraction of blue HBs increases with the distance from the Galactic center. Measuring the metallicities, colours and luminosities of stars in these clusters is hampered by many difficulties, such as high visual extinction, differential reddening, crowding and contamination from field stars.

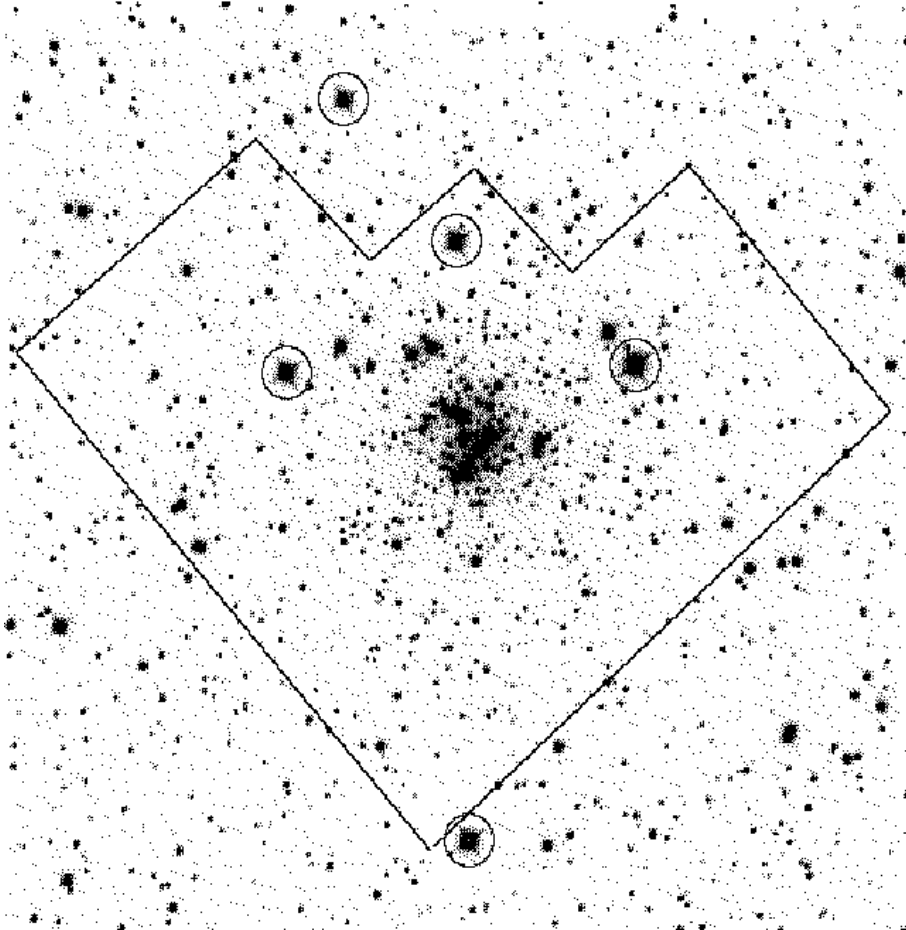
Send offprint requests to: Y. Momany

<sup>★</sup> Based on data collected at La Silla; ESO programs: 64.N-0645(A), 65.L-0610(A), and HST archival data

Optical Colour-Magnitude Diagrams (CMDs) of metal rich GCs are characterized by the extended turnover of the

**Table 1.** Journal of observations of NGC 6528

Type	Filter	No. of Im.	DIT×NDIT	FWHM	$X$	$\Delta m$
DEEP	$J$	3	10×6	0.78	1.408	0.080
DEEP	$H$	3	10×6	0.78	1.366	0.085
DEEP	$K_s$	3	5×12	0.75	1.328	0.086
SHALLOW	$J$	3	1.18×10	0.91	1.493	0.076
SHALLOW	$H$	3	1.18×10	0.91	1.467	0.081
SHALLOW	$K_s$	3	1.18×10	0.85	1.443	0.079

**Fig. 1.** A  $3'6 \times 3'6$  section of the *DEEP*  $K$  mosaic image of NGC 6528. North is to the left, East is to the bottom. The field of view of the HST observations is outlined. Also marked are the 5 candidate variables stars (see text).

Red Giant Branch (RGB) caused by TiO blanketing effects, especially strong in the  $V$  band (Ortolani et al. 1990, 1991; Heitsch & Richtler 1999). Combining data from optical and Near-Infrared (NIR) allows one to investigate the dependence of stellar properties on colour better than relying on that of optical or NIR data alone (Cohen et al. 1978; Kuchinski et al. 1995; Guarnieri et al. 1998; Ferraro et al. 2000, hereafter F00).

NIR data have the great advantage of having small bolometric corrections for cool stars, since they bracket the spectral region of maximum stellar flux density (Frogel et al. 1980; Cohen et al. 1981). This allows a straightforward comparison with theoretical models.

NGC 6528 is among the best studied metal rich GCs of the galactic bulge. HST/WFPC2 observations showed that the CMD of this cluster is virtually identical to that of the bulge GC NGC 6553, and that the age of these two clusters is the same as halo GCs within a  $\sim \pm 20\%$  (systematic) uncertainty (Ortolani et al. 1995).

Recent distance estimates put the cluster within  $\leq 1$  kpc from the Galactic center (Barbuy et al. 1998). Both optical (Ortolani et al. 1995; Richtler et al. 1998) and IR studies (Cohen & Sleeper 1995; Ferraro et al. 2000; Ortolani et al. 2001) agree that it is among the most metal rich clusters. Although the metal abundance estimates in the literature span a  $\sim 0.6$  dex, all values are in the metal rich regime. This wide range in metal-

**Table 2.** NGC 6528 metallicity estimates from literature

Method	[Fe/H]	[M/H]	Ref.
$Q_{39}$ index		+0.1	Zinn & West (1984)
optical diagrams		solar	Ortolani et al. (1992)
		-0.20	Barbuy et al. (1998)
			Ferraro et al. (2000)
IR Ca II integrated spectra	-0.38 <sup>a</sup>		Armandroff & Zinn (1988)
IR abs. at 1.6 $\mu\text{m}$	-0.23		Origlia et al. (1997)
NIR diagrams		+0.10	Cohen & Sleeper (1995)
IR Ca triplet equivalent widths	-0.33		Rutledge et al. (1997)
low resolution spectra	-0.50	-0.25	Coelho et al. (2001)
high resolution spectra	+0.07		Carretta et al. (2001)

<sup>a</sup> on the Carretta & Gratton (1997) scale calibration.

licity is partly due to uncertainties in the reddening towards NGC 6528. Values in the literature span a very wide range: e.g.  $E_{B-V} = 0.45$  (Richtler 1998),  $E_{B-V} = 0.50$  (Carretta et al. 2001),  $E_{B-V} = 0.52$  (Barbuy et al. 1998),  $E_{B-V} = 0.55$  (Ortolani et al. 1992),  $E_{B-V} = 0.73$  (Reed et al. 1988), up to  $E_{B-V} = 0.77$  (Schlegel et al. 1998) in the cluster direction.

Ortolani et al. (2001) presented HST/NICMOS  $JH$  CMDs for NGC 6528, reaching 3 magnitudes below the turn-off, and derived an age of  $13 \pm 3$  Gyr. Their NIR diagrams are also as “clean” as the optical diagrams of Feltzing et al. (2002), who used two epochs of HST/WFPC2 images to proper-motion decontaminate stars of NGC 6528 from those belonging to the Galactic bulge.

In this paper a new NIR data set of NGC 6528 is presented. The  $5 \times 5$  arcmin<sup>2</sup>  $JHK_s$  observations allow the construction of NIR CMDs that better sample the RGB and reach close to the turnoff. We also proper-motion decontaminate the HST  $VI$  set, extracting a cleaned  $VJHK$  sample. Based on this wider colour baseline we derive new reddening and distance estimates, and check calibrations of photometric metallicity indicators.

In Sect. 2 the  $JHK$  and archival HST data are presented. Section 3 highlights the reduction procedures for both data sets. The original and cleaned NIR CMDs are presented in Sect. 4, while in Sect. 5 the HB and RGB bump luminosities are derived. In Sect. 6 reddening and distance modulus estimates towards NGC 6528 are derived. In Sect. 7 we derive the metallicity of NGC 6528 based on various calibrations of the RGB morphology. Lastly, Sect. 9 summarizes our results.

## 2. Observations

### 2.1. NIR Observations

The observations were carried out on two different runs at the ESO NTT telescope: on 2000, February 20–21 and July 2–3. Both runs used the SOFI infrared camera equipped with a Hawaii HgCdTe  $1024 \times 1024$  pixels array detector. The image scale of  $0''.29$  pixel was used for

all observations, yielding a field of view of  $4'.9 \times 4'.9$ . The read-out mode was Double Correlated Read (DCR). This yielded a readout noise of 2.1 ADU and a gain of 5.53 electrons/ADU. Observations of the first run were conducted under photometric conditions and a seeing of less than  $\sim 0.8$  arcsec, whereas the second run had variable seeing conditions, up to 1.5 arcsec. These observations were taken with two different exposures times: DEEP to reach the fainter stars at acceptable S/N, and SHALLOW to allow the sampling of bright RGB/AGB stars.

In Table 1 the journal of observations is presented. Columns 1 and 2 refer to the type of images taken and the filters used. Column 3 (No. of Im) stands for the number of dithered images. Column 4 gives the DIT  $\times$  NDIT (Detector Integration Time and Number of Detector Integration Time, respectively). Columns 5, 6 and 7 give the stellar FWHM (in arcsec), the airmass, and the derived aperture correction. The numbers reported in Cols. 5, 6 and 7 refer to the final stacked image. Figure 1 shows a  $\sim 3'.6 \times 3'.6$   $K$  mosaic image, corresponding to a section of the entire DEEP field, upon which the field of view of the HST observations is outlined.

The DEEP images of NGC 6528 were taken in sets of six images: 3 dithered images were centered on the object and 3 images, centered in an adjacent region, were dedicated to sky sampling. The dithering steps were of the order of  $4''.0$ . Standard stars from Persson et al. (1998) were also observed on a regular basis at airmasses comparable with those of the target object. For each standard star five measurements were obtained: 4 measurements having the star centered in the 4 quadrants of the detector and one with the star in the center of the detector.

### 2.2. HST Observations

Two sets of archive WFPC2 HST observations, GO5436 and GO8696, separated by 6.093 years are used. Our goal was to use a proper-motion cleaned  $VI$  data set to decontaminate our  $JHK$  photometry. Feltzing et al. (2002) used the same data to proper-motion decontaminate the optical CMD of NGC 6528. We therefore refer the reader

to their work for a detailed presentation of the two sets of observations.

### 3. Data reduction

#### 3.1. Pre-reduction

The pre-reduction of the NIR data consists of (1) dark frame subtraction, (2) sky subtraction and (3) flat fielding of both scientific and standard star frames. We basically applied the reduction steps given in the SOFI manual (Lidman et al. 2000) to which the reader is referred for a detailed presentation. In the process of flatfielding the illumination correction frames and the bad pixels maps, both available from the ESO webpages, were used.

A typical  $J$  sequence consisted of 3 scientific images and 3 sky images. We scaled the sky images to a common median after rejecting the highest and lowest pixels. On the other hand, a typical standard star sequence already contains information about its local sky, as most of the array in fact measures the sky. Hence, at no additional cost in observing time, a median combination of the standard stars sequences automatically gave their local sky frames.

Finally, both target and standard star images had their associated sky subtracted and were divided by their respective flatfields. At this point, these images were cleaned using the bad pixels maps. To create the combined images of the object, scientific images were aligned by applying standard IRAF tasks. The matching and coaddition of the individual images was facilitated by the presence of many bright stellar sources, and the offsets were determined accurately.

#### 3.2. Calibration

##### 3.2.1. Standard Stars

The photometric calibrations were defined using 4 standard stars from Persson et al. (1998), namely 9106, 9119, 9143, 9172 and the red star LHS 2397a. Their Table 3 showed that, for red stars,  $K_s$  and  $K$  are rarely different by more than 0.02: the average difference is 0.0096 mag, with a standard deviation of 0.017 mag. We therefore assume that the use of the  $K_s$  filter instead of the  $K$  filter introduces an extra uncertainty in the photometric calibration of this filter of  $\pm 0.02$  mag (see also Ivanov et al. 2000). Standard star curves of growth, obtained with the IRAF/APPHOT task, showed that a radius of 18 pixels (5.2 arcsec) gave a satisfactory convergence of aperture photometry for all the standards. This is consistent with the fact that Persson et al. (1998) used an aperture of 10 arcsec in diameter.

The study of Montegriffo et al. (1995) has shown the existence of some spatial variation in the photometric response of IR cameras. We checked this possibility and found no significant variations in the 5 measurements of standard stars. In the process of calibrating the standard stars, the 5 aperture photometry measurements were averaged.

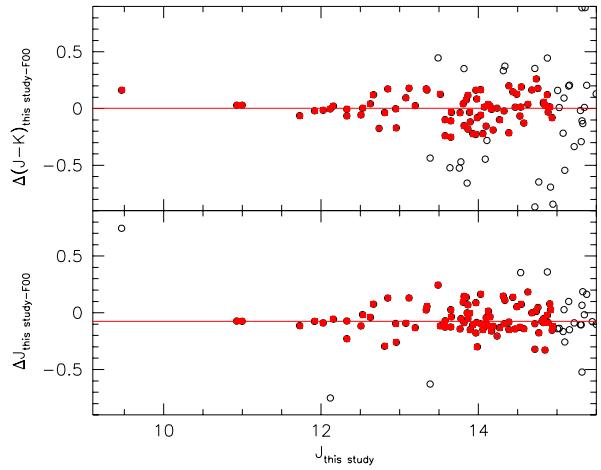


**Fig. 2.** A comparison between our  $JK$  data of NGC 6528 and those of F00. The horizontal line marks the median differences after applying a  $1\sigma$  rejection (filled circles).

The instrumental magnitudes of the standards were normalized to 1s exposure and zero airmass, according to the following equation:

$$m' = m_{\text{ap}} + 2.5 \log(t_{\text{exp}}) - K_{\lambda} X \quad (1)$$

where  $m_{\text{ap}}$  is the mean instrumental magnitude of the 5 measurements in a circular aperture of radius  $R = 5.2$  arcsec,  $X$  is the mean airmass and  $t_{\text{exp}}$  is the DIT in seconds. The mean extinction coefficients adopted for La Silla are:  $K_J = 0.10$ ,  $K_H = 0.04$  and  $K_{K_s} = 0.05$  (from ESO webpages). A least squares fit of the normalized instrumental magnitudes to the magnitudes of Persson et al. (1998) gave the following relations:

$$J - j = +0.004 \times (J - H) + 23.089 \quad (2)$$

$$H - h = +0.032 \times (J - H) + 22.888 \quad (3)$$

$$K - k_s = -0.001 \times (J - K) - 22.346 \quad (4)$$

The r.m.s. scatter of the residuals of the fit is 0.041, 0.020, and 0.021 mag in  $J$ ,  $H$  and  $K$  respectively. Accounting for the uncertainty in the use of the  $K_s$  filter instead of the  $K$  filter, we therefore assume that 0.04, 0.02 and 0.03 represent our calibration uncertainties in  $J$ ,  $H$  and  $K$  bands respectively.

##### 3.2.2. Calibrated Catalogues

We made use of the DAOPHOT II and ALLSTAR (Stetson 1987, 1994) packages for stellar photometry. After running the FIND and PHOT tasks, we searched for isolated stars to build the PSF for each of the final images. These PSF candidates showed no faint components and the subtraction turned out to be smooth. The final PSF were generated with a PENNY function that had a quadratic dependence on position in the frame. The photometry was finally performed on the stacked images using ALLSTAR.

The instrumental photometric catalogues contain PSF magnitudes. These were converted into aperture magnitudes assuming that  $m_{\text{ap}} = m_{\text{PSF}} - \text{constant}$  (Stetson 1987), where the constant is the aperture correction to be found. The aperture corrections were estimated as in the optical case: bright isolated stars were selected in each field and had their neighbours (within 5.8 arcsec radius) subtracted, then aperture magnitudes were measured through increasing circular apertures with radii within  $R = 3.5 - 5.8$  arcsec. The curves of growth of the brightest stars showed a satisfactory aperture photometry convergence at a radius of 18 pixels (5.2 arcsec), the same as for the standard stars. The aperture corrections are reported in Col. 7 of Table 1. Having estimated the aperture corrections, calibrated magnitudes were obtained by applying Eqs. 2–4, and the final DEEP and SHALLOW catalogues of NGC 6528 were produced.

All catalogues in the same passband were then matched. For stars in common, we computed the error-weighted mean of the magnitude differences. Note that the SHALLOW and DEEP catalogues (for each passband) overlap over an interval of  $\sim 5$  magnitudes, and that the magnitude differences did not exceed 0.03 mag. At this point, the mean of the magnitude differences was applied to the SHALLOW catalogues so as to share the same magnitude scale of the DEEP ones. Stars found *only* in either catalogues are flagged and included anyhow in the final catalogue, whereas those found in both SHALLOW and DEEP were recorded with their DEEP magnitudes, that have a higher signal to noise. Finally, a *JHK* colour catalogue is produced by associating the entries of the combined single passband catalogues described above.

### 3.3. Comparison with Previous Photometry

Ferraro et al. (2000) presented a homogenous NIR database of 10 Galactic GCs, obtained at the ESO/MPI 2.2 m telescope equipped with the NIR camera IRAC-2. A bright star sample of NGC 6528 was matched with the photometry of Ferraro et al., kindly provided by the authors. The panels of Fig. 2 show the results of a comparison of our photometry with the Ferraro et al. sample; applying a  $1\sigma$  rejection yielded the following values:  $\Delta J_{\text{this study-F00}} = -0.076 \pm 0.110$  and  $\Delta(J-K)_{\text{this study-F00}} = 0.003 \pm 0.120$ . The differences in the *J* and *K* scales are of the order of the uncertainties of the aperture corrections, and overall show the excellent consistency of the two magnitude scales.

### 3.4. HST reduction and proper-motion decontamination

The methods used to reduce the HST WFPC2 archive observations are similar to those employed by Anderson & King (2000) and will not be further commented here. Instead, we briefly comment on the methods used to derive a cleaned CMD. To carry out the astrometry, the

algorithms of Anderson & King (2000) based on the *effective* point-spread function (PSF) were used. The basis of the method is to determine a finely sampled PSF of high accuracy from images at dithered offsets. The fitting of this PSF to individual images gives a positional accuracy of the order of  $\sim 0.02$  pixels, showing no systematic error arising from the location of the star with respect to the pixel boundaries. Since all astrometric measurements were made with respect to reference stars that are cluster members, the zero point of motion is the centroid motion of the cluster (King et al. 1998; Bedin et al. 2001).

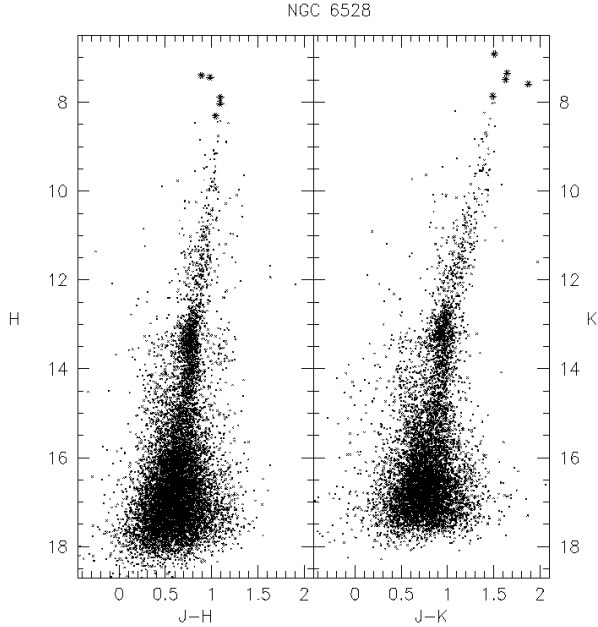
It is important to note that for stars brighter than  $V \sim 16.8$  ( $K \sim 12$ ), the core of the PSF is flattened due to saturation, and this is where most of the astrometric information is contained (WFPC2 is severely undersampled). Therefore, any tentative decontamination of cluster stars brighter than ( $K \sim 12$ ) is hampered by saturation. Besides saturations effects, many bright stars in our *JHK* sample are not included in the decontamination process because they lie outside the HST field of view or do not have *VI* counterparts within 1 pixel matching radius.

The decontamination process resulted in *VI* diagrams, that are very similar to those obtained by Feltzing et al. (2002). We therefore use their same cuts on the retrieved stellar proper motion in the *l* and *b* coordinates, i.e.  $\sqrt{\mu_l^2 + \mu_b^2} < 0''.09$  for  $V \geq 19$  and  $\sqrt{\mu_l^2 + \mu_b^2} < 0''.23$  for  $V < 19$ . Lastly, the decontaminated *VI* data were used to extract a *cleaned VJHK* sample of NGC 6528 stars. For the rest of this paper by *cleaned* diagram we refer to the product of imposing the above cuts.

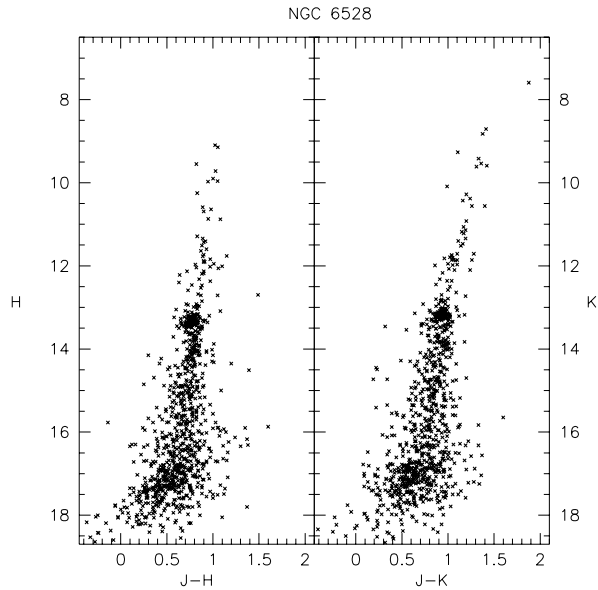
## 4. The Colour-Magnitude Diagrams

Figure 3 presents the *H, J - H* and *K, J - K* diagrams of the observed field towards NGC 6528 (only stars with DAOPHOT errors less than 0.08 mag have been plotted). This figure shows the CMDs originating from the whole  $5 \times 5$  arcmin<sup>2</sup> SOFI field. The wide cluster coverage has the side effect of high contamination by bulge stars that outnumber those of the cluster. Note that NGC 6528 is well inside the Galactic bulge and its metallicity (listed in Table 2) is close to the mean value for bulge stars ( $[\text{Fe}/\text{H}] = -0.25$ ; McWilliam & Rich 1994, hereafter MR94). Therefore one expects the main features of the CMD (RGB, HB and MS) to be populated by both the cluster and bulge populations (in addition to the disk contamination). On the other hand, the diagrams show a well sampled, almost vertical, RGB sequence spanning from  $K \simeq 16.5$  to  $K \simeq 7.0$ . The present photometry is also deep enough to reach the cluster’s subgiant branch.

Figure 4 displays the corresponding decontaminated CMDs, which refer to the much smaller HST field where the astrometric decontamination was conducted. Hence, the decrease in the number of RGB stars in the lower panels is not only due to the decontaminating process but also to limitation of the WFPC2 field of view. The cleaned *JHK* data, and the subsequent matching with the HST



**Fig. 3.** The original  $H, J - H$  and  $K, J - K$  colour-magnitude diagrams of NGC 6528. Only stars with DAOPHOT errors less than 0.08 have been plotted. Starred symbols are the candidate variable stars (see text).



**Fig. 4.** As above but for the decontaminated diagrams.

$V$  data provide the basis for our further analysis of the cluster's parameters.

In Fig. 5 we show the dereddened (see Sect. 6 for the adopted reddening and distance)  $(J - H)_0, (H - K)_0$  two colour diagram. The overplotted loci are those by Bessell & Brett (1988) for carbon stars and long period variables (long-dashed), and Frogel et al. (1978) for variables with  $P > 350$  d (dotted). The mean locus for K and M giants by Bessell & Brett (1988) is also plotted (solid line). This figure clearly shows that most stars in our sample are K

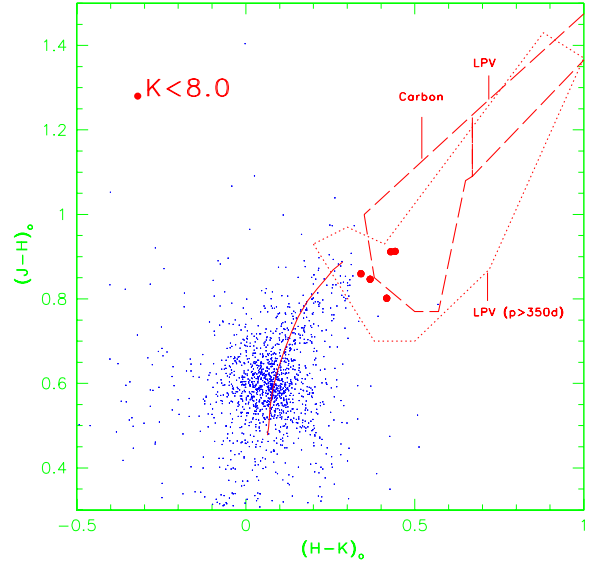


**Fig. 5.** The dereddened  $(J - H)_0, (H - K)_0$  two colour diagram of NGC 6528. The overplotted loci are those by Bessell & Brett (1988) for carbon stars and long period variables (long-dashed), and Frogel et al. (1978) for variables with  $P > 350$  d (dotted). The mean locus for K and M giants by Bessell & Brett (1988) is also plotted (solid line).

and M giants. Moreover, that a number of stars have IR colours typical of carbon and long period variable stars. Among these we plot as filled circles stars with  $K < 8.0$  ( $M_{bol}^{tip} \simeq -3.6$ ), and cautiously argue that these have the highest probability of being AGB stars (also plotted as starred symbols in Figs. 3 and 5). As shown by Frogel et al. (1990), all stars brighter than  $M_{bol} = -3.6$  are exclusively AGB objects, while fainter than this limit they are mostly RGB objects. This interpretation is in good agreement with the estimated RGB tip of NGC 6528 being at  $M_{bol}^{tip} = -3.68$  (F00). However, in the absence of spectroscopic confirmation and given the difficulties explained in Sect. 3.4, we can not firmly establish the cluster membership of these variable candidates.

## 5. The HB and the RGB bump

The brightness and amplitude of the RGB bump are metallicity dependent, becoming stronger and fainter as metallicity increases (F00). Therefore the identification of the RGB bump can be used to derive relative metallicities. Following the methods described in Fusi Pecci et al. (1990), the upper panel of Fig. 6 shows the cumulative logarithmic  $K$  luminosity function (LF) of a decontaminated RGB sample. The dashed lines are linear fits to the regions above and below the bump and highlight the change in the slope of the RGB cumulative LF. The vertical line marks the RGB bump that we identify at  $K_{Bump}^{NGC 6528} = 13.85 \pm 0.05$ . This value is 0.2 mag brighter

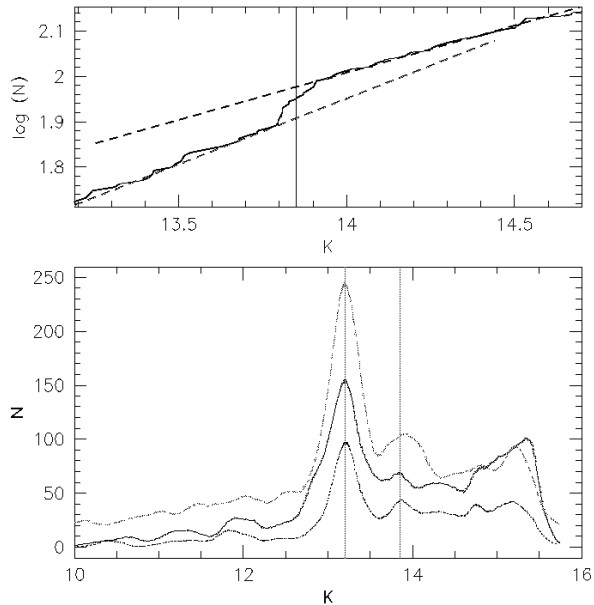


**Fig. 6.** The upper panel shows the cumulative logarithmic  $K$  luminosity function of a cleaned RGB sample. The dashed lines are linear fits to the regions above and below our estimated location of the bump, marked by the vertical line. The lower panel shows a multi-bin, multi-interval, smoothed differential LF of (1) NGC 6528 original data (solid line); (2) NGC 6528 *cleaned* data (dotted line); and (3) NGC 6553 original data (dashed line) by Guarneri et al. (1998). Solid vertical lines mark the estimated location of the RGB bump and HB in NGC 6528.

than that found by F00, and in good agreement with the value of  $K = 13.80$  derived by Davidge (2000).

The lower panel of Fig. 6 presents 3 multi-bin, multi-interval, smoothed differential LFs of (1) NGC 6528, original data (solid line); (2) NGC 6528, *cleaned* data (dotted line); and (3) NGC 6553, original data (dashed line) by Guarneri et al. (1998), shifted to the distance and reddening of NGC 6528. Following Bedin et al. (2000), these curves were constructed in a way to reduce the effects of statistical fluctuations, the assumed interval in the  $K$  magnitudes, or the assumed bin size. We first allowed the bin size to vary between 0.10 and 0.50 in steps of 0.01 mag. Then, and for each of the 40 bins, different LFs were constructed by changing the starting  $K$  magnitude interval. The distribution of these LFs (sharing the same bin size but not the same  $K$  interval) was used to assign a *single* LF for that particular bin size. Finally, the 40 LFs were normalized and smoothed.

The most conspicuous feature in Fig. 6 is the peak marking the HB level. The *cleaned* and original NGC 6528 data show an excellent agreement on the HB being at  $K = 13.20 \pm 0.05$ . The second notable feature is the RGB bump. The *cleaned* NGC 6528 curve shows this feature at  $K = 13.85$ , in perfect agreement with that derived from the cumulative LF. Also, Fig. 6 shows how NGC 6528

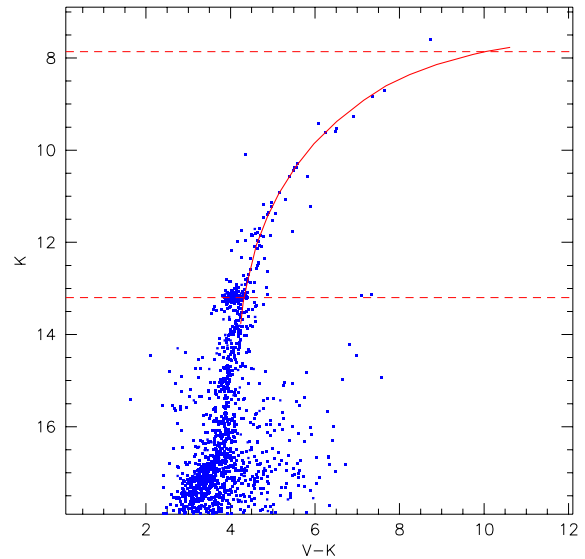


**Fig. 7.** The *cleaned*  $K, V - K$  diagram of NGC 6528 along with the shifted fiducial line (solid curve) of NGC 6553 (Guarneri et al. 1998). The dashed lines mark the HB and the RGB tip of NGC 6553, which coincide perfectly with their counterparts in NGC 6528.

**Table 3.** Summary of the comparison between the CMDs of NGC 6553 and NGC 104 with respect to NGC 6528

NGC	$\Delta$ colour	$\Delta$ mag	$E_{B-V}$	$(m - M)_{\odot}$
6553	$\Delta(J - K) = -0.03$	$\Delta K = 0.78$	0.64	14.38
6553	$\Delta(V - K) = -0.35$	$\Delta K = 0.78$	0.57	14.38
104	$\Delta(J - K) = +0.36$	$\Delta J = 1.20$	0.44	14.55

and NGC 6553 share essentially the same separation between the HB and RGB bump levels. This confirms earlier evidence of the similar metallicity of the two objects (Ortolani et al. 1995).

## 6. Reddening & distance

The interstellar reddening and distance of NGC 6528 was estimated by comparing its CMDs with the fiducial lines of NGC 6553 in various planes. Also, a similar comparison was done with respect to NGC 104 (47 Tuc). The CMDs of NGC 6528 are, in fact, almost identical to those of NGC 6553 (Ortolani et al. 1995). This is best shown in Fig. 7 which displays the *cleaned*  $K, V - K$  diagram of NGC 6528 along with the shifted fiducial line of NGC 6553 (Guarneri et al. 1998). The dashed lines mark the HB and RGB tip of NGC 6553 from Guarneri et al. (1998).

The results of the comparison between the CMDs of NGC 6528 and those of NGC 6553 and NGC 104 are reported in Table 3, in which Col. 2 and 3 refer to colour and magnitude shifts applied to the comparison cluster in order to match the CMD of NGC 6528. The last two

columns report the derived values of  $E_{B-V}$  and  $(m-M)_\odot$ . In this comparison we assumed:

- $E_{B-V} = 0.70$  and  $(m-M)_\odot = 13.60$  for NGC 6553 (Guarnieri et al. 1998);
- $E_{B-V} = 0.04$ ,  $(m-M)_\odot = 13.32$ , and  $[\text{Fe}/\text{H}] = -0.71$  for NGC 104 (F00);
- $A_V = 3.1 \times E_{B-V}$ ;
- the reddening law of Rieke & Lebofsky (1985).

When shifting the RGB fiducial line of NGC 104 with respect to NGC 6528, one must keep in mind that part of the colour shift is due to the different metallicities of the two clusters. We accounted for this effect by using two isochrones from the Marigo & Girardi (2001) library to estimate the  $J-K$  colour difference of the two isochrones at the HB level. This value was found to be  $\sim 0.11$  mag, and was subtracted from the  $J-K$  colour difference reported in Table 3.

The mean of the reddening values reported in Table 3 is  $E_{B-V}^{\text{NGC6528}} = 0.55$ , and we will adopt this value for the rest of the paper. This reddening value is intermediate when compared to the values reported in the literature, ranging from  $E_{B-V} = 0.45$  (Richtler et al. 1998) up to  $E_{B-V} = 0.77$  (Schlegel et al. 1998). It is also consistent with that inferred from Carretta et al. (2001) who estimate a mean excitation equilibrium temperature of 4 red-HB stars to be  $T_{\text{eff}} \sim 4610$  K, yielding to  $E_{B-V} = 0.50$ . Note however that excitation temperatures suffer deviations from local thermodynamic equilibrium (NLTE) effects on FeI lines, and give systematically higher values than photometric temperature (Thévenin & Idiart 1999), therefore this does not give a strong constraint on the reddening value. A discussion on the  $E_{B-V}$  of NGC 6528 using integrated spectra is given in Bruzual et al. (1997). From the spectral energy distribution of NGC 6528, they derive  $E_{B-V} = 0.62$ .

The derived mean distance modulus of NGC 6528 is  $(m-M)_\odot = 14.44$  (7.7 kpc), i.e. 0.05 larger than that obtained by Ortolani et al. (1992). An independent check on the mean distance modulus was obtained from the  $K$  mean luminosity of the HB level, using the Guarnieri et al. (1998) calibration. Guarnieri et al. (1998) observed six globular clusters with metallicities in the range  $-2.3 < [\text{Fe}/\text{H}] < -0.14$ , and determined  $M_K^{\text{HB}} = -0.20[\text{Fe}/\text{H}] - 1.53$ , where  $[\text{Fe}/\text{H}]$  is on the Zinn & West (1984, hereafter ZW) scale. Assuming  $[\text{Fe}/\text{H}]_{\text{ZW}}^{\text{NGC6528}} = -0.20$  (see Sect. 7.2), we derive  $M_K^{\text{HB}} = -1.49$ . From the measured mean level of the HB,  $K_{\text{HB}} = 13.20$ , and adopting an extinction  $A_K = 0.193$ , we therefore obtain a distance modulus  $(m-M)_\odot = 14.50$ . This value is only 0.06 mag larger than the value obtained from the CMD fitting.

## 7. Metallicity

In Table 2 we report literature metallicity values assigned to NGC 6528. In discussions about metallicity values, it is important to distinguish between  $[\text{Fe}/\text{H}]$  and

$[\text{M}/\text{H}]$ . Strictly,  $[\text{Fe}/\text{H}] = \log(\text{Fe}/\text{H})_* - \log(\text{Fe}/\text{H})_\odot$  is the iron abundance, as commonly derived from the numerous Fe I and Fe II lines available in high resolution spectra.  $[\text{M}/\text{H}]$  gives the abundance of metals; if some elements are in excess relative to Fe,  $[\text{M}/\text{H}]$  has to be computed taking into account these excesses.  $Z$  is further weighted by the mass of the elements, but in  $[Z]$  (more usually indicated by  $[Z/Z_\odot]$ ) the masses are cancelled, such that  $[Z] = [\text{M}/\text{H}]$ . Isochrones are calibrated in terms of  $Z$ . Ultimately, both photometric measurements and isochrone determination depend on a calibration to be given in terms of  $[\text{Fe}/\text{H}]$ , which is the primary calibrator (since it is directly measured from spectra).

The RGB morphology in the CMDs of globular clusters is a powerful metallicity indicator, due to its strong dependence on continuum and line blanketing by heavy elements, and essentially no dependence on helium abundance and age. The behaviour of the RGB morphology in the optical was discussed by Ortolani et al. (1991), and in the infrared by Kuchinski et al. (1995) and F00. It is worth mentioning that the slope in the  $K, V-K$  CMD is far more sensitive to metallicity than in a fully IR CMD (e.g.  $K, J-K$ ). In the following section, we analyze a number of features that characterize the RGB morphology and are used as photometric metallicity indicators.

### 7.1. RGB slope

In the  $K, J-K$  plane, Kuchinski & Frogel (1995) investigated the behaviour of the RGB slope in metal rich GCs ( $-1.0 < [\text{Fe}/\text{H}] < -0.3$ ), and found that the slope ( $S_{\text{RGB}}$ ) of a linear fit to RGB stars brighter than the HB can be used to estimate the metallicity with an accuracy of  $\pm 0.25$  dex. The importance of this metallicity indicator relies on the fact that it is reddening and distance independent. Following their indications, we selected stars from 0.6 to 5.1 mag above the HB level on the *cleaned*  $K, J-K$  diagram of NGC 6528. Since the method is very sensitive to small variations in the adopted slope, special care was needed in eliminating cluster HB stars and field stars. We found that a variation of 0.01 in the slope translates into a change in the estimated metallicity of about  $\sim 0.2$  dex. We derive a slope of  $-0.109$  from the *cleaned* CMDs. Using the Kuchinski & Frogel (1995) calibration this corresponds to  $[\text{Fe}/\text{H}] = -0.38$  on the ZW scale.

### 7.2. Other $[\text{Fe}/\text{H}]$ indicators

Ferraro et al. (2000) presented a homogeneous NIR database of 10 globular clusters spanning a wide metallicity range. Analyzing the RGB morphology they calibrated a variety of observables as metallicity indicators (RGB slope, RGB  $J-K$  and  $V-K$  colours at different magnitude levels, and RGB  $K$  magnitudes at different colours), and based their calibrations on the Carretta & Gratton (1997, hereafter G97) metallicity scale. Columns 1 and 2 in Table 4 report the applied F00 calibrations and



**Table 4.** Metallicity estimates based on the F00 calibrations of RGB slope, and RGB specific colours and magnitudes

Metallicity indicator	$[\text{Fe}/\text{H}]_{\text{CG97}}$	$^a [\text{Fe}/\text{H}]_{\text{ZW}}$	$^b [\text{Fe}/\text{H}]_{\text{CCGB01}}$
$M_K^{(J-K)_\circ=0.7}$	-0.10	-0.12	+0.27
$M_K^{(V-K)_\circ=3.0}$	+0.01	-0.19	+0.10
$(J-K)_\circ^{M_K=-5.5}$	-0.04	-0.17	+0.15
$(J-K)_\circ^{M_K=-5.0}$	+0.02	-0.14	+0.22
$(V-K)_\circ^{M_K=-5.5}$	-0.29	-0.27	-0.08
$(V-K)_\circ^{M_K=-5.0}$	-0.27	-0.23	+0.01
$\text{Log } T_{\text{eff}}^{\text{bump}}$	-0.17	-0.19	+0.10
$M_{\text{bol}}^{\text{bump}}$	-0.14	-0.18	+0.12
RGB slope	-0.42	-0.18	+0.12
$^c$ RGB slope	-0.38	-0.32	-0.18
$^d M_K^{\text{Bump}}$	-0.42		

<sup>a</sup> our calibration of the F00 data on the ZW scale

<sup>b</sup> values in Col. 3 transformed onto the CCGB01 scale

<sup>c</sup> based on the Kuchinski & Frogel (1995) calibration

<sup>d</sup> based on the Cho & Lee (2002) calibration

their corresponding  $[\text{Fe}/\text{H}]_{\text{CG97}}$  estimates. All these values were obtained on the the *cleaned*  $J-K$ ,  $V-K$  and  $M_{\text{bol}}$ ,  $\log(T_{\text{eff}})$  diagrams. Besides, we use the Cho & Lee's (2002)<sup>1</sup> calibration of the RGB bump, identified in 11 GCs (based on data from the 2MASS point source catalogue).

The CG97 scale, however, has been revised by Carretta et al. (2001, CCGB01) based on high-dispersion spectroscopy of NGC 6528 and NGC 6553. In order to provide metallicity estimates on the new CCGB01 scale and on the widely used scale of ZW, we use the tables of F00 to (1) re-calculate the F00 calibrations on the ZW scale (Col. 3 in Table 4), and (2) place these latter values onto the CCGB01 scale (Col. 4), by applying equation 3 in Carretta et al. (2001). Averaging the values of Col. 3 yields  $[\text{Fe}/\text{H}]_{\text{ZW}} = -0.20$ , while the average of Col. 4 gives  $[\text{Fe}/\text{H}]_{\text{CCGB01}} = +0.08$ , and we will adopt these values as our best estimates. Similarly, by applying various F00 calibrations of the global metallicity, we derive a mean value  $[\text{M}/\text{H}] \approx 0.0$ . Indeed, the expected  $[\text{M}/\text{H}]$  value should be  $\sim 0.2$  dex higher than  $[\text{Fe}/\text{H}]$  if the overabundance of  $\alpha$ -elements in NGC 6528 is similar to that of bulge stars (e.g., MR94).

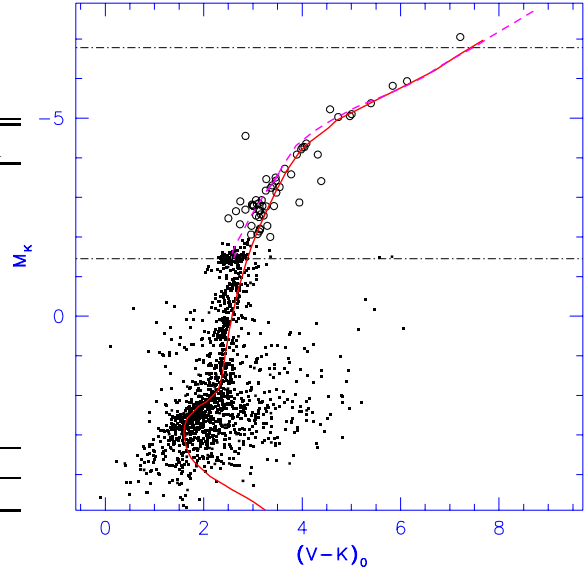


**Fig. 8.** The *cleaned*  $M_K$ ,  $(V-K)_\circ$  diagram of NGC 6528 assuming  $E_{B-V}^{\text{NGC6528}} = 0.55$  and  $(m-M)_\circ = 14.44$ . Superimposed is a theoretical isochrone from Bertelli et al. (1994) with 12.6 Gyr and  $Z = 0.02$ . A dashed line highlights the HB and AGB phases. The horizontal lines mark the HB and RGB tip location. Stars with  $M_K < -2$  were drawn with different symbols for more visibility with respect to the isochrone.

### 7.3. Isochrone fitting

Figure 8 shows the *cleaned*  $M_K$ ,  $(V-K)_\circ$  diagram of NGC 6528 with a 12.6 Gyr and  $Z = 0.02$  theoretical isochrone from Bertelli et al. (1994). The best fit was obtained applying our values for reddening and distance,  $E_{B-V} = 0.55$  and  $(m-M)_\circ = 14.44$ . An even higher global metallicity of  $Z = 0.04$  was found by Feltzing et al. (2002) by using the  $\alpha$ -enhanced isochrones of Salasnich et al. (2000). Adopting these latter isochrones to fit our  $K$ ,  $V-K$  diagrams would result in an extremely high metallicity of  $Z = 0.07$ . These isochrone would reconcile only with the highest estimates of metallicity from spectroscopy, such as those by Carretta et al. (2001); we believe that the colours of these isochrones may be systematically too blue.

## 8. The $M_{\text{bol}}$ , $\log(T_{\text{eff}})$ diagram

In Fig. 9 we show the NGC 6528 data in the  $M_{\text{bol}}$ ,  $\log(T_{\text{eff}})$  plane. Since the decontamination process strongly affects

<sup>1</sup> As pointed out by Carpenter (2001), the Persson et al. (1998) standards (used in this paper) have been adopted as the fiducial calibrator in 29 of the 35 2MASS calibration fields, thereby connecting the zero points of the 2MASS to the Las Campanas Observatory (LCO) photometric system. Hence, a roughly zero photometric offset is expected in the 2MASS-LCO transformation equations. This is confirmed by Carpenter's equation 22.

the brightest portion of the RGB (due to the combined effects of saturation in the HST  $V$  data and the smaller HST field of view), we plot both the cleaned  $K, V - K$  diagram (left panel) and the original  $K, J - K$  data (right panel). Candidate AGB variables are plotted as starred symbols. The observed CMD was converted into the  $M_{\text{bol}}, \log(T_{\text{eff}})$  plane by using Table 4 of Montegriffo et al. (1998) to derive transformations in terms of the  $V - K$  and  $J - K$  colours. The bolometric corrections and effective temperature scales were obtained by Montegriffo et al. as a function of NIR-optical colours, using a large data base of giants in GCs with  $-2.0 < [\text{Fe}/\text{H}] < 0.0$ . Using the cleaned diagram, we computed two of the F00 metallicity indicators namely,  $\text{Log } T_{\text{eff}}^{\text{bump}}$  and  $M_{\text{bol}}^{\text{bump}}$  (Table 4).

Although the membership of the variable AGB candidates is still to be confirmed spectroscopically, it is interesting to note the analogy with the bolometric magnitudes of the confirmed long period variables in NGC 6553, where the brightest star is found at  $M_{\text{bol}} \simeq -4.7$ . Guarnieri et al. (1997) discussed the maximum AGB luminosity as an age indicator, and used the NIR data of NGC 6553 (Guarnieri et al. 1998) as a template for the metal rich component of external galaxies. Interestingly, they found that the brightest stars in NGC 6553 were as bright as the brightest AGB stars in the dwarf elliptical galaxy M32. Thus, the metal rich population of NGC 6553, which is as old as the Galactic halo GCs, is able to generate stars as bright as those observed in M32. This clearly shows that an “intermediate age” (few to several Gyr) is not needed to account for the brightest stars in external galaxies such as M32.

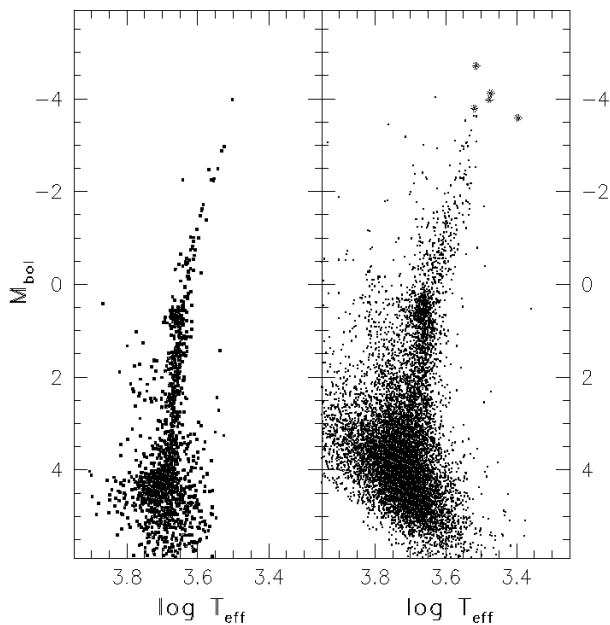


**Fig. 9.** The left panel shows the *cleaned*  $K, V - K$  data in the  $M_{\text{bol}}, \log(T_{\text{eff}})$  theoretical plane. Right panel shows the original  $K, J - K$ . Starred symbols are the candidate AGB variables.

## 9. Summary and conclusions

We have presented new high-quality NIR observations of the Galactic globular cluster NGC 6528. The  $JHK_s$  data allow the construction of deep NIR CMDs reaching the subgiant branch. Moreover, as in Feltzing et al. (2002), we proper-motion decontaminate the HST  $V$  set to extract a clean  $VJHK$  sample. Based on this wider colour baseline set, and on a comparison with the CMDs of NGC 6553 and NGC 104, we derive new reddening and distance estimates for NGC 6528:  $E_{B-V} = 0.55$  and  $(m - M)_o = 14.44$  (7.7 kpc).

We also test various calibrations of photometric metallicity indicators. Averaging the results from 10 metallicity indicators we derive a mean value of  $[\text{M}/\text{H}] \approx 0.0$  for NGC 6528. The best isochrone fit to our cleaned  $K, V - K$  diagram is obtained adopting a 12.6 Gyr and  $Z = 0.02$  isochrone from Bertelli et al. (1994). Thus, we conclude that the metallicity of NGC 6528 is very close to the mean of field stars of Baade’s Window,  $[\text{Fe}/\text{H}] = -0.25$ , as derived by MR94.

Although the membership of five AGB variable candidates is still to be confirmed spectroscopically, these are bolometrically as bright as the confirmed long period variables in NGC 6553 and M32. As discussed in Guarnieri et al. (1997), this may imply that an “intermediate age” (few Gyr old) component is not needed to account for the brightest stars in external galaxies such as M32.

*Acknowledgements.* We thank the anonymous referee for helpful remarks that improved the presentation of this paper. We also thank Dr. Ferraro for providing us their RGB fiducial lines and data, and Dr. Carretta for useful discussions.

## References

- Anderson, J., & King, I. R. 2000, PASP, 112, 1360
- Armandroff, T. E. & Zinn, R. 1988, AJ, 96, 92
- Barbuy, B., Bica, E., Ortolani, S. 1998, A&A, 333, 117
- Barbuy, B., Ortolani, S., Bica, E., Desidera, S. 1999, A&A, 348, 783
- Bedin, L. R., Piotto, G., Zoccali, M., Stetson, P. B., Saviane, I., Cassisi, S., & Bono, G. 2000, A&A, 363, 159
- Bedin, L. R., Anderson, J., King, I. R., & Piotto, G. 2001, ApJ, 560, L75
- Bertelli, G., Bressan, A., Chiosi, C., Fagotto, F., & Nasi, E. 1994, A&AS, 106, 275
- Bessell, M. S., & Brett, J. M. 1988, PASP, 100, 1134
- Bruzual, G., Barbuy, B., Ortolani, S., Bica, E., Cuisinier, F., Lejeune, T., Schiavon, R.P., 1997, AJ, 114, 1531
- Carpenter, J. M. 2001, AJ, 121, 2851
- Carretta, E., & Gratton, R. G. 1997, A&AS, 121, 95 (CG97)
- Carretta, E., Cohen, J. G., Gratton, R. G., & Behr, B. B. 2001, AJ, 122, 1469 (CCGB01)
- Cho, D., & Lee, S., 2002, AJ, 124, 977
- Coelho, P., Barbuy, B., Perrin, M.-N., Idiart, T., Schiavon, R. P., Ortolani, S., & Bica, E. 2001, A&A, 376, 136
- Cohen, J. G., Persson, S. E., & Frogel, J. A. 1978, ApJ, 222, 165
- Cohen, J. G., Persson, S. E., Elias, J. H., & Frogel, J. A. 1981, ApJ, 249, 481

- Cohen, J. G., & Sleeper, C. 1995, *AJ*, 109, 242
- Davidge, T. J. 2000, *ApJS*, 126, 105
- Feltzing, S., Johnson, R. A., & de Cordova, A. 2002, *A&A*, 385, 67.
- Ferraro, F. R., Montegriffo, P., Origlia, L., & Fusi Pecci, F. 2000, *AJ*, 119, 1282 (F00)
- Frogel, J. A., Persson, S. E., Matthews, K., & Aaronson, M. 1978, *ApJ*, 220, 75
- Frogel J. A., Persson S. E., Cohen J. G. 1980, *ApJ*, 239, 495
- Frogel, J. A., Mould, J., & Blanco, V. M. 1990, *ApJ*, 352, 96
- Fusi Pecci, F., Ferraro, F. R., Crocker, D. A., Rood, R. T., & Buonanno, R. 1990, *A&A*, 238, 95
- Guarnieri, M. D., Ortolani, S., Montegriffo, P., Renzini, A., Barbuy, B., Bica, E., & Moneti, A. 1998, *A&A*, 331, 70
- Guarnieri, M. D., Renzini, A., & Ortolani, S. 1997, *ApJ*, 477, L21
- Heitsch, F., & Richtler, T. 1999, *A&A*, 347, 455
- Ivanov V.D., Borissova J., Alonso-Herrero A., Russeva T., 2000, *AJ*, 119, 2274
- King, I. R., Anderson, J., Cool, A. M., & Piotto, G. 1998, *ApJ*, 492, L37
- Kuchinski, L. E., Frogel, J. A., Terndrup, D. M., & Persson, S. E. 1995, *AJ*, 109, 1131
- Kuchinski, L. E., & Frogel, J. A. 1995, *AJ*, 110, 2844
- Lidman, C., Cuby, J-G., & Vanzi, L. 2000, in "SOFI user's manual" Doc. No. LSO-MAN-ESO-40100-0003, issue 13
- McWilliam, A., & Rich, R. M. 1994, *ApJS*, 91, 749 (MR94)
- Marigo, P., & Girardi, L. 2001, *A&A*, 377, 132
- Montegriffo, P., Ferraro, F. R., Fusi Pecci, F., & Origlia, L. 1995, *MNRAS*, 276, 739
- Montegriffo, P., Ferraro, F. R., Origlia, L., & Fusi Pecci, F. 1998, *MNRAS*, 297, 872
- Origlia, L., Ferraro, F. R., Fusi Pecci, F., & Oliva, E. 1997, *A&A*, 321, 859
- Ortolani, S., Barbuy, B., Bica, E. 1990, *A&A*, 236, 362
- Ortolani, S., Barbuy, B., Bica, E. 1991, *A&A*, 249, L31
- Ortolani, S., Bica, E., & Barbuy, B. 1992, *A&AS*, 92, 441
- Ortolani, S., Renzini, A., Gilmozzi, R., Marconi, G., Barbuy, B., Bica, E., & Rich, R. M. 1995, *Nature*, 377, 701
- Ortolani S., Barbuy B., Bica E., Renzini A., Zoccali M., Rich R.M., Cassisi S. 2001, *A&A*, 376, 878
- Persson, S. E., Murphy, D. C., Krzeminski, W., Roth, M., & Rieke, M. J. 1998, *AJ*, 116, 2475
- Reed, B. C., Hesser, J. E., & Shawl, S. J. 1988, *PASP*, 100, 545
- Richtler, T., Grebel, E. K., Subramaniam, A., & Sagar, R. 1998, *A&AS*, 127, 167
- Rieke, G. H. & Lebofsky, M. J. 1985, *ApJ*, 288, 618
- Rutledge, G. A., Hesser, J. E., & Stetson, P. B. 1997, *PASP*, 109, 907
- Salasnich, B., Girardi, L., Weiss, A., & Chiosi, C. 2000, *A&A*, 361, 1023
- Schlegel, D. J., Finkbeiner, D. P., & Davis, M. 1998, *ApJ*, 500, 525
- Stetson P. B., 1987, *PASP*, 99, 191
- Stetson P.B., 1994, *PASP*, 106, 250
- Thévenin, F., & Idiart, T. 1999, *ApJ*, 521, 753
- Zinn, R., & West, M. J., 1984, *ApJS*, 55, 45 (ZW)